

Observing quantum state diffusion by heterodyne detection of fluorescence

P. Campagne-Ibarcq,^{1,2} P. Six,^{3,2} L. Bretheau,^{1,2} A. Sarlette,² M. Mirrahimi,² P. Rouchon,^{3,2} and B. Huard^{1,2,*}

¹*Laboratoire Pierre Aigrain, Ecole Normale Supérieure-PSL Research University,
CNRS, Université Pierre et Marie Curie-Sorbonne Universités,*

Université Paris Diderot-Sorbonne Paris Cité, 24 rue Lhomond, 75231 Paris Cedex 05, France

²*Quantic Team, INRIA Paris-Rocquencourt, Domaine de Voluceau, B.P. 105, 78153 Le Chesnay Cedex, France*

³*Centre Automatique et Systèmes, Mines ParisTech, PSL Research University,
60 Boulevard Saint-Michel, 75272 Paris Cedex 6, France.*

(Dated: August 28, 2015)

A qubit can relax by fluorescence, which prompts the release of a photon into its electromagnetic environment. By counting the emitted photons, discrete quantum jumps of the qubit state can be observed. The succession of states occupied by the qubit in a single experiment, its quantum trajectory, depends in fact on the kind of detector. How are the quantum trajectories modified if one measures continuously the amplitude of the fluorescence field instead? Using a superconducting parametric amplifier, we have performed heterodyne detection of the fluorescence of a superconducting qubit. For each realization of the measurement record, we can reconstruct a different quantum trajectory for the qubit. The observed evolution obeys quantum state diffusion, which is characteristic of quantum measurements subject to zero point fluctuations. Independent projective measurements of the qubit at various times provide a quantitative validation of the reconstructed trajectories. By exploring the statistics of quantum trajectories, we demonstrate that the qubit states span a deterministic surface in the Bloch sphere at each time in the evolution. Additionally, we show that the sole monitoring of fluorescence can generate coherences out of classical states. Counterintuitively, measuring light emitted during relaxation can give rise to trajectories with increased excitation probability.

I. INTRODUCTION

The quantum properties of an open system are preserved as long as no information about its state is lost into unmonitored degrees of freedom [1]. For a qubit, the mere possibility to emit a photon by spontaneous emission can lead to decoherence. When discarding the information carried by the emitted field, the imperfectly known qubit state is described by a density matrix, which evolves continuously towards the ground state. If instead an observer monitors the fluorescence light emitted by the qubit, the lost information is retrieved. The succession of states occupied by the qubit then depends on the particular realization of the random measured record and deviates from the average one [2–4].

Peculiar to quantum mechanics, this quantum trajectory depends on the type of detection. In case of photocounting, the qubit undergoes discrete quantum jumps as already observed on single ions in the 1980’s [5–7]. In contrast Wiseman and Milburn showed in 1992 that heterodyne measurement of fluorescence should lead to continuous quantum state diffusion [8, 9]. Here, we perform such a measurement on a superconducting qubit using a phase-preserving parametric amplifier [10, 11], which ensures an overall measurement efficiency $\eta = 24\%$ for the qubit relaxation channel. Without drive and starting from an initially pure state, we demonstrate that the qubit state evolves erratically towards the ground

state $|g\rangle$, in agreement with quantum state diffusion [9]. The validity of the obtained quantum trajectories is verified using an independent tomographic measurement. Counterintuitively, the sole monitoring of relaxation can temporarily increase the probability amplitude of excitation [12]. It can also generate coherences out of classical states, which is in contrast with the recently observed quantum trajectories based on quantum non demolition measurement of the qubit [13–17].

In the experiment sketched in Fig. 1a, the qubit under monitoring is a transmon resonating at $f_q = 6.37$ GHz. It is dispersively coupled to a 3D bulk copper cavity [19, 20], which serves two purposes. First, it channels most of the emission coming from qubit relaxation into a dominantly coupled output transmission line [21]. The qubit decay rate is measured to be $\gamma_1 = (4.15 \mu\text{s})^{-1}$. Second, it can be used to perform a projective readout of the qubit [18, 22] that will be used as a validation of the quantum trajectories in section III. At time $t = 0$, the qubit is prepared either in the excited state $|e\rangle$ or in $|+x\rangle = \frac{1}{\sqrt{2}}(|g\rangle + |e\rangle)$. This is done by applying a rotation pulse (Fig. 1b) on the qubit initially at equilibrium, where its excitation is below 1 % consistently with dilution refrigerator temperatures. The qubit is then left to decay while heterodyne detection of the fluorescence field is performed on the output line using a high efficiency detection setup based on a Josephson Parametric Converter (JPC) [11, 18, 23].

*Electronic address: benjamin.huard@ens.fr

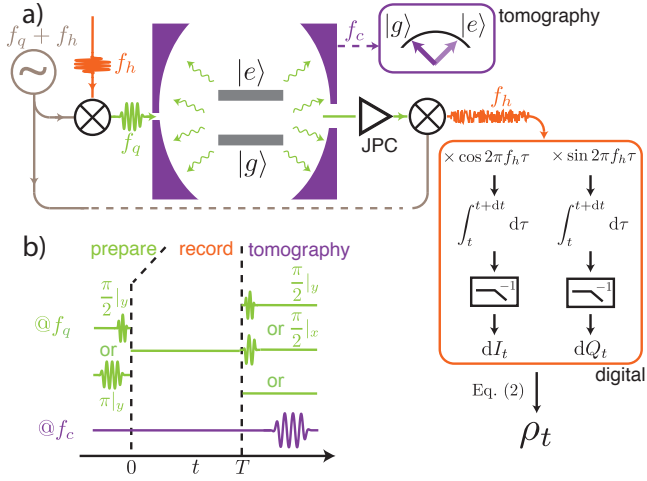


Figure 1: **Scheme of the experiment.** **a)** The fluorescence field of a superconducting qubit in an off-resonant cavity is recorded using a heterodyne detection setup from time 0 to T . Following amplification by a Josephson Parametric Converter (JPC), the signal is downconverted to $f_h = 100$ MHz and numerically demodulated and integrated on time steps $dt = 200$ ns into its two quadratures dI and dQ . The rectangular symbols represent the correction of finite detection bandwidth in the setup [18]. The quantum trajectory $\{\rho_t\}$ is then computed using Eq. (2). A single local oscillator at $f_q + f_h$ is used for qubit manipulation and downconversion of the fluorescence signal. The transmission at cavity frequency $f_c = 7.8$ GHz is used to independently readout the qubit at time T [18]. **b)** Pulse sequence. At time 0, the qubit is prepared in $|+x\rangle$ (resp. $|+e\rangle$) with a 52 ns (resp. 104 ns) rotation pulse around σ_y . The fluorescence record is acquired for a duration T ranging from 0 to 10 μ s. The state is then projectively readout along one of the three Pauli operators using a pulse at frequency f_c preceded by a rotation pulse around σ_y , σ_x , or no pulse.

II. COMPUTING QUANTUM TRAJECTORIES FROM HETERODYNE MEASUREMENT OF FLUORESCENCE

Previous experiments on superconducting circuits have shown that the fluorescence field contains a footprint of the qubit state [24–27]. Indeed, the integrated outputs dI_t and dQ_t of an heterodyne detector between times t and $t + dt$ are on average proportional to $\langle \sigma_x \rangle_{\rho_t} = \text{Tr}(\rho_t \sigma_x)$ and $\langle \sigma_y \rangle_{\rho_t}$ respectively, where ρ_t is the density matrix of the qubit and $\sigma_{x,y,z}$ the Pauli operators. In the inset of Fig. 2a is shown in blue the average of 3 millions measurement records $\{dI_t, dQ_t\}_{0 < t < T}$ for a qubit starting in $|+x\rangle$. As expected, the quadrature dI_t decays exponentially at a rate $\gamma_1/2 + \gamma_\phi$ while the quadrature dQ_t is zero. We note that the pure dephasing rate $\gamma_\phi \approx (35 \mu\text{s})^{-1}$ is measured to be much smaller than γ_1 . Two individual measurement records are shown in Fig. 2a for a qubit starting in $|+x\rangle$ and in Fig. 2c when starting in $|e\rangle$. They are fluctuating with a much larger amplitude than the average signal. This noise originates both from

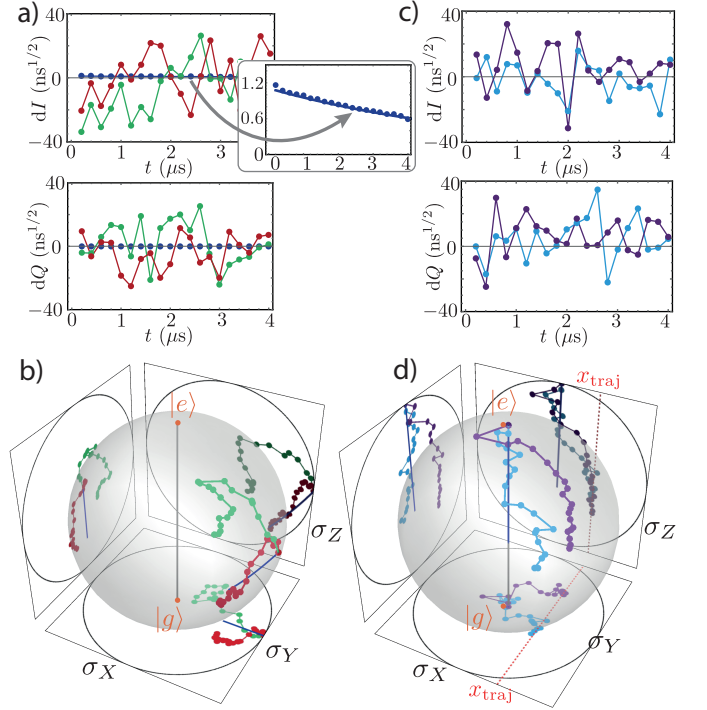


Figure 2: **Quantum trajectories.** **a)** Each panel displays two different measurement records of one quadrature of the fluorescence field for a qubit initially in $|+x\rangle$. Actual measurements are shown as red and green dots linked by straight lines for clarity. The blue dots correspond to the average record on all experiments, and the blue line corresponds to an exponential fit of these dots in $e^{-\gamma_1 t/2 - \gamma_\phi t}$. A zoom in is shown as an inset. **b)** Quantum trajectories followed by the qubit under relaxation represented in the Bloch sphere for the measurement records shown in Fig. 2a. The Bloch vector (x, y, z) corresponds to the state $\rho = (\mathbf{1} + x\sigma_x + y\sigma_y + z\sigma_z)/2$ and the black circles set the scale of the Bloch sphere extrema. The trajectories are obtained by solving numerically Eq. (2) and are shown as dots linked by straight lines both in the sphere and in the three projections along x , y and z . Colors identify which record of Fig. 2a is used. A blue line shows the average evolution without monitoring ($\eta = 0$). **c,d)** Same representations for two realizations starting from $|e\rangle$. They were arbitrarily selected to end up in a state with similar Bloch coordinate $x_{\text{traj}} = 0.42 \pm 0.02$ as indicated by a dashed red line.

zero point fluctuations of the detected field quadratures, which contain information on the qubit state, and from imperfections of the detection setup. The relative contribution of the first one is characterized by the efficiency η . Using the record $\{dI_t, dQ_t\}_{0 < t < T}$ and the initial state ρ_0 , one can reconstruct a quantum trajectory $\{\rho_t\}$ over the time T . The density matrix ρ_t is here conditioned to the knowledge of the initial state at time 0 and of the fluorescence record between 0 and t .

Mathematically, the measurement records can be de-

composed as [3]

$$\begin{cases} dI_t = \sqrt{\frac{\eta\gamma_1}{2}} \langle \sigma_x \rangle_{\rho_t} dt + dW_{I,t} \\ dQ_t = \sqrt{\frac{\eta\gamma_1}{2}} \langle \sigma_y \rangle_{\rho_t} dt + dW_{Q,t} \end{cases} \quad (1)$$

where $dW_{I,t}$ and $dW_{Q,t}$ are the random fluctuations beyond the expected average value. The signals are normalized so that the variance of dI_t and dQ_t is directly dt . The overall efficiency $\eta = 24\%$ is determined using a max-like method [28]. It is limited by both the extra relaxation mechanisms that do not lead to emission into the output line and limited efficiency of the detection setup. The evolution of the density matrix can be inferred from these measurement records using the following Stochastic Master Equation. In the frame rotating at f_q , and without qubit drive, it reads [3, 29]

$$\begin{aligned} d\rho_t = & (\gamma_1 \mathcal{D}[\sigma_-]\rho_t + \gamma_\phi/2 \mathcal{D}[\sigma_z]\rho_t) \times dt \\ & + \sqrt{\eta\gamma_1/2} \mathcal{M}[\sigma_-]\rho_t \times dW_{I,t} \\ & + \sqrt{\eta\gamma_1/2} \mathcal{M}[i\sigma_-]\rho_t \times dW_{Q,t}, \end{aligned} \quad (2)$$

using the Lindblad $\mathcal{D}[L]\rho = L\rho L^\dagger - \frac{1}{2}L^\dagger L\rho - \frac{1}{2}\rho L^\dagger L$ and measurement $\mathcal{M}[L]\rho = (L - \langle L \rangle_\rho)\rho + \rho(L - \langle L \rangle_\rho)^\dagger$ super-operators and the lowering operator $\sigma_- = |g\rangle\langle e|$.

When fluorescence is not monitored, which can be modeled by setting the measurement efficiency to zero, the qubit state dynamics is captured by the deterministic Lindblad terms. The first one corresponds to the average effect of relaxation, while the second one models pure dephasing and is almost negligible here. The corresponding evolution of the Bloch vector is plotted in blue in Figs. 2b,d.

By monitoring fluorescence during relaxation ($\eta > 0$), the observer retrieves part of the information lost in the environment. The acquired information is injected in Eq. (2) solely via the noise terms $dW_{I,t}$ and $dW_{Q,t}$. The associated stochastic quantum backaction is captured by $\mathcal{M}[\sigma_-]$ and $\mathcal{M}[i\sigma_-]$ of Eq. (2) (see [18, 30] for a graphical representation of backaction in the Bloch sphere). It is then possible to reconstruct the quantum trajectory of the qubit corresponding to a measurement record. In practice, we choose a time step $dt = 200$ ns close to the autocorrelation time induced by the finite bandwidth of the detection setup [18]. This limited sampling rate still enables an accurate estimation of the trajectory using a discrete time version of Eq. (2) [18, 31, 32]. The quantum trajectories originating from the measurement records in Fig. 2a,c are represented in Fig. 2b,d. They present an erratic behavior coming from the randomness of the measurement backaction yet eventually converge towards $|g\rangle$ (south pole). This is similar to a random walk in the Bloch sphere with a step size that decreases to zero as the state approaches $|g\rangle$. Strikingly, the trajectories differ from the average one owing to a large enough measurement efficiency $\eta = 24\%$. If the detection was ideal ($\eta = 1$) and without pure dephasing, the state would remain pure and the Bloch vector would evolve stochastically on the surface of the Bloch sphere.

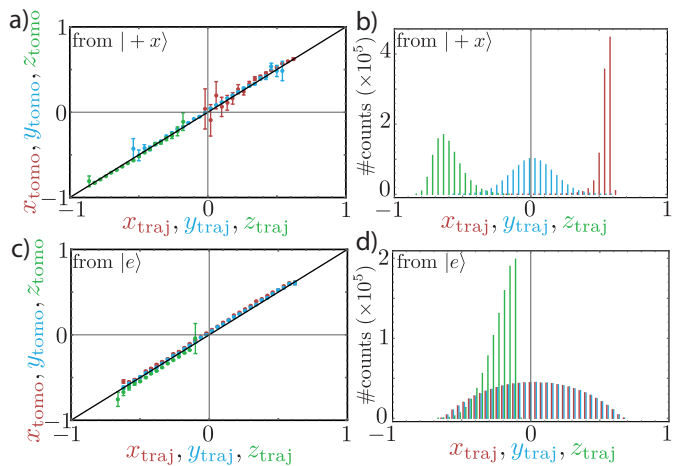


Figure 3: **Tomography versus quantum trajectories.** **a)** For each value of x_{traj} , a red dot indicates the average value x_{tomo} of the final measurement of σ_x on the subset of experiments starting from $|+x\rangle$ and for which the quantum trajectory ends up at time $T = 4 \mu\text{s}$ in a state such that $\langle \sigma_x \rangle_{\rho_T} = x_{\text{traj}} \pm 0.02$. Error bars represent the statistical uncertainty and the solid line has a slope 1. Subsets with less than 40 experiments are not shown. The final projective measurement infidelity is corrected for [18]. Similar dots represent the case of y (blue) and z (green). **b)** Distribution of the final Bloch coordinate x_{traj} of the 10^6 quantum trajectories starting in $|+x\rangle$ for $T = 4 \mu\text{s}$, and followed by a σ_i projective measurement. The color code and the bin width match those in Fig. 3a. **c-d)** Same as **a-b** for experiments starting in $|e\rangle$.

III. VALIDATION OF THE QUANTUM TRAJECTORIES BY INDEPENDENT MEASUREMENTS

Using Eq. (2), we are able to reconstruct the quantum trajectories corresponding to an initial state at time 0 and a fluorescence record between 0 and T . By nature, the final state ρ_T encodes the statistics of any measurement that would take place at time T . In order to test the pertinence of this prediction, independent measurements are performed for T ranging from 1 to 10 μs . A projective measurement of the qubit is thus performed, following a $\pi/2$ pulse around σ_y or around σ_x , or no pulse at all (Fig. 1b). The experiment is repeated one million times for each final measurement of σ_x , σ_y or σ_z , for each preparation and for each final time T .

In the case of a final measurement of σ_x , we then select the subset of all the realizations whose final predicted Bloch coordinate $\langle \sigma_x \rangle_{\rho_T}$ ends up within 2% of a given value x_{traj} . The test then consists in comparing x_{traj} to the mean value x_{tomo} of the final σ_x measurement outcome on that subset. The tomography results match the predictions of Eq. (2) as can be seen in Fig. 3a, where we plot in red x_{tomo} as a function of x_{traj} for the $T = 4 \mu\text{s}$ -long trajectories starting in $|+x\rangle$. Similar measurements are shown for the σ_y and σ_z measurements in the same figure. The error bars represent

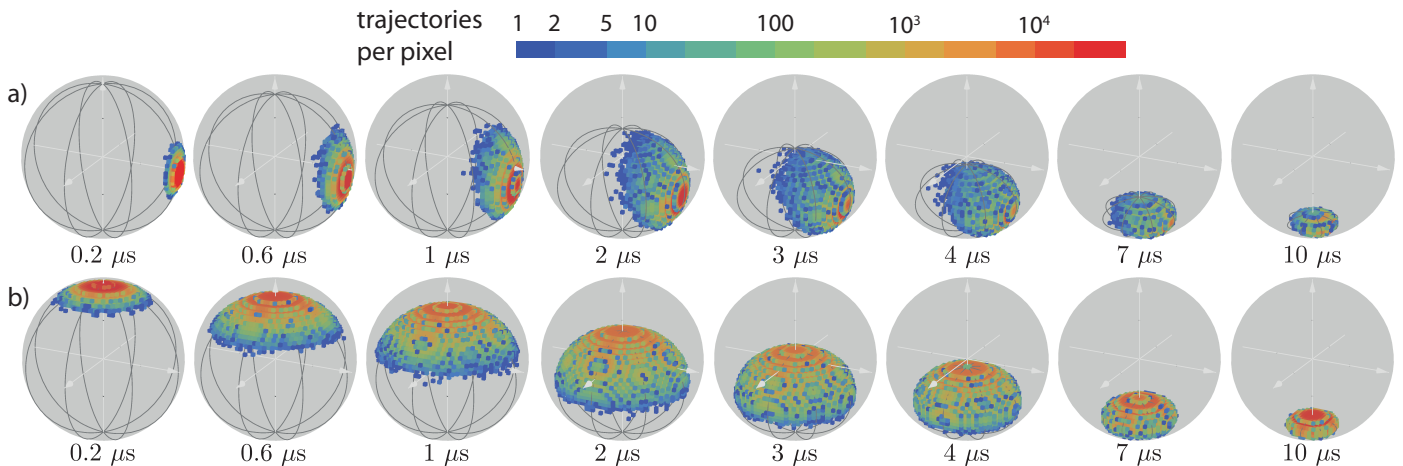


Figure 4: **Statistics of quantum trajectories.** Distributions of the qubit states along 10 μs -long trajectories for a qubit initially in $|+x\rangle$ (a) and $|e\rangle$ (b). The number of trajectories reaching each cubic cell of side 0.04 is encoded in color, out of a total of 3 millions. White arrows go from -1 to $+1$ along $\sigma_{x,y,z}$ and the Bloch sphere is colored in gray. Meridians of the spheroid spanned by Eq. (5) are also shown.

the statistical uncertainty on x_{tomog} corresponding to the limited number of selected realizations for a given x_{traj} plotted in Fig. 3b [18]. The same verification is realized on experiments starting from $|e\rangle$ (Figs 3c,d). Slight constant offsets between the predicted (*traj*) and tomography (*tomo*) values appear. The fact that these offsets are larger when the qubit starts in $|e\rangle$ than in $|+x\rangle$ indicates that they originate from systematic errors in the initial qubit preparation. Note that there is no fit parameter in the model beside η [28]. The agreement between the states reconstructed using the fluorescence signal and the ones measured through tomography is also good for all other considered times T (not shown here).

IV. STATISTICS OF QUANTUM TRAJECTORIES

Now that the approach is validated, the experiment can be used to probe the statistics of quantum trajectories. Fig. 3b,d represent the distribution of predicted states at time $T = 4 \mu\text{s}$. The average of each Bloch coordinate matches its expected value after a relaxation of $4 \mu\text{s}$. The spread of the distributions comes from measurement backaction. Starting from $|e\rangle$ (Fig. 3d), the qubit state has no defined initial phase, and this symmetry is preserved: $\langle\sigma_x\rangle_{\rho_T}$ and $\langle\sigma_y\rangle_{\rho_T}$ remain 0 on average. However, at the single realization level, coherences develop in time by spontaneous symmetry breaking due to the inherent randomness of the measurement process. This is in sharp contrast with the quantum trajectories obtained by continuous dispersive measurement of σ_Z [13] when starting from a classical state.

The statistics of quantum trajectories can be better understood in the Bloch sphere representation. In Fig. 4, is represented the distribution of the qubit states at various

times t for 10 μs -long trajectories, for a qubit starting in $|+x\rangle$ (a) or $|e\rangle$ (b). Starting from a single point, the state distribution progressively spreads out and collapses down to $|g\rangle$ at long times. Note that at the first times in the evolution, the distribution spread in the Bloch sphere is larger when starting from $|e\rangle$ than from $|+x\rangle$. This illustrates that the measurement backaction associated with spontaneous emission is as strong as the qubit excitation is large. Strikingly, at each time in the evolution, all quantum states seem to belong to the same shell in the Bloch sphere, independently of the initial state.

An analytical expression of this surface can in fact be derived when neglecting dephasing ($\gamma_\phi = 0$ in Eq. (2)). Let us introduce the variable

$$\alpha = 1 + \frac{1}{2} \frac{S_L}{p_e^2} \geq 1, \quad (3)$$

where, $S_L = 1 - \text{Tr}(\rho_t^2)$ is the linear entropy and $p_e = (1 + \langle\sigma_z\rangle_{\rho_t})/2$ is the probability to find the qubit excited. It can then be shown [18] that $\alpha(t)$ evolves deterministically, independently of the heterodyne fluorescence record, following

$$\alpha(t) = \eta + (\alpha(0) - \eta)e^{\gamma t}. \quad (4)$$

Remarkably, the qubit state does not diffuse stochastically in the volume of the Bloch sphere. Rather, it is restricted to the surface determined by the value $\alpha(t)$ whose characteristic equation reads

$$\alpha(x^2 + y^2) + \alpha^2(z + 1 - \frac{1}{\alpha})^2 = 1. \quad (5)$$

The surface is thus a spheroid going through the south pole of the Bloch sphere $|g\rangle$. Starting from a pure state at $\alpha = 1$, the spheroid shrinks from the Bloch sphere itself towards the south pole as α rises in time. As shown

in Fig. 4, it is in good agreement with the measured distributions. The small thickness [18] of the shell in Fig. 4 originates from pure dephasing alone. Note that in the ideal case $\eta = 1$, the trajectories would evolve on the sphere as $\alpha(t) = 1$ is then constant.

On the spheroid, the evolution is still stochastic and depends on the particular realization of the heterodyne measurement of fluorescence. Yet, it is possible to identify integral quantities of the measured quadratures $\{dI_t, dQ_t\}$ alone that relate directly to the position on the spheroid, hence avoiding to solve numerically Eq. (2). For that purpose, the position of a state on the spheroid is parametrized by the variables $\xi_x(t) = \frac{\langle \sigma_x \rangle_{\rho_t}}{\langle \sigma_z \rangle_{\rho_t} + 1}$ and $\xi_y(t) = \frac{\langle \sigma_y \rangle_{\rho_t}}{\langle \sigma_z \rangle_{\rho_t} + 1}$. We show that [18]

$$\begin{cases} \xi_x(t) = \xi_x(0)e^{\gamma t/2} + \sqrt{\frac{\eta\gamma_1}{2}} \int_0^t e^{\gamma_1(t-\tau)/2} dI_\tau \\ \xi_y(t) = \xi_y(0)e^{\gamma t/2} + \sqrt{\frac{\eta\gamma_1}{2}} \int_0^t e^{\gamma_1(t-\tau)/2} dQ_\tau \end{cases} \quad (6)$$

These expressions can be tested using the same tomography measurements as in Fig. 3 and lead to a similar agreement [18].

For some trajectories in Fig. 4a starting from $|+x\rangle$, the probability for the qubit to be excited increases in time as $\langle \sigma_z \rangle_{\rho_\tau}$ temporarily takes positive values. This is counterintuitive as the average energy increases for a subset of experiments that can be postselected based on the field emitted during decay [12]. This observation makes explicit the inadequacy of a reasoning in terms of emitted photons in the case of heterodyne or homodyne detection. In contrast, any signal detected by a photo counter would be associated with decreasing qubit energy. A trajectory with increasing $\langle \sigma_z \rangle$ is shown in Fig. 2a and results from a measurement record that starts with negative values of dI_t over some time interval while the qubit state is still close to $|+x\rangle$.

V. CONCLUSION

Quantum state diffusion was first introduced as a description of what an open quantum system undergoes

from the viewpoint of its environment [8]. This experiment, which implements the proposal of Wiseman and Milburn in 1992 [3, 9], illustrates how it can in fact be understood as the dynamics of a system conditioned to a continuous measurement record. In that respect, it provides new insight about how to understand relaxation and decoherence. The use of a Josephson Parametric Converter was instrumental in order to reach a high enough measurement efficiency so that measurement backaction is visible and quantum trajectories depart from their average. Importantly, it was possible to validate the reconstructed quantum trajectories by an independent quantum state tomography. The experiment thus demonstrates how the sole continuous monitoring of a relaxation channel can lead to various quantum states and even produce superpositions of classical ones. It opens the way to experiments in which the field emitted during relaxation is used as an input of a feedback controller able to stabilize any state of a qubit [30]. This would complement the toolbox of quantum error correction, which is key to the development of quantum computing. Finally, the possibility to observe statistics of quantum trajectories should lead to interesting perspectives in the field of thermodynamics of quantum information.

Acknowledgments

We thank Alexia Auffèves, Maxime Clusel, Pascal Degiovanni, Michel Devoret, Emmanuel Flurin, François Mallet and Vladimir Manucharyan for fruitful discussions. Nanofabrication has been made within the consortium Salle Blanche Paris Centre. This work was supported by the EMERGENCES grant QUMOTEL of Ville de Paris and by the IDEX program ANR-10-IDEX-0001-02 PSL*.

-
- [1] W. Zurek. *Classical selection and quantum Darwinism*. *Physics Today* **68**, 9–10 (2015).
 - [2] H. Carmichael. *Quantum trajectory theory for cascaded open systems*. *Physical review letters* **70**, 2273 (1993).
 - [3] H. M. Wiseman and G. J. Milburn. *Quantum measurement and control* (Cambridge University Press, 2009).
 - [4] A. Barchielli and M. Gregoratti. *Quantum Trajectories and Measurements in Continuous Time*, vol. 782 (Springer-Verlag Berlin Heidelberg, 2009).
 - [5] J. Bergquist, R. Hulet, W. Itano and D. Wineland. *Observation of Quantum Jumps in a Single Atom*. *Physical Review Letters* **57**, 1699–1702 (1986).
 - [6] W. Nagourney, J. Sandberg and H. Dehmelt. *Shelved optical electron amplifier: Observation of quantum jumps*. *Physical Review Letters* **56**, 2797–2799 (1986).
 - [7] T. Sauter, W. Neuhauser, R. Blatt and P. Toschek. *Observation of quantum jumps*. *Physical Review Letters* **57**, 1696–1698 (1986).
 - [8] N. Gisin and I. C. Percival. *The quantum-state diffusion model applied to open systems*. *Journal of Physics A: Mathematical and General* **25**, 5677 (1992).
 - [9] H. M. Wiseman and G. J. Milburn. *Interpretation of quantum jump and diffusion processes illustrated on the Bloch sphere*. *Physical Review A* **47**, 1652–1666 (1993).

- [10] N. Bergeal, F. Schackert, M. Metcalfe, R. Vijay, V. Manucharyan, L. Frunzio, D. Prober, R. Schoelkopf, S. Girvin and M. Devoret. *Phase-preserving amplification near the quantum limit with a Josephson ring modulator*. Nature **465**, 64–68 (2010).
- [11] N. Roch, E. Flurin, F. Nguyen, P. Morfin, P. Campagne-Ibarcq, M. H. Devoret and B. Huard. *Widely Tunable, Nondegenerate Three-Wave Mixing Microwave Device Operating near the Quantum Limit*. Physical Review Letters **108**, 147701 (2012).
- [12] A. Bolund and K. Mølmer. *Stochastic excitation during the decay of a two-level emitter subject to homodyne and heterodyne detection*. Phys. Rev. A **89**, 023827 (2014).
- [13] K. Murch, S. Weber, C. Macklin and I. Siddiqi. *Observing single quantum trajectories of a superconducting quantum bit*. Nature **502**, 211–214 (2013).
- [14] M. Hatridge, S. Shankar, M. Mirrahimi, F. Schackert, K. Geerlings, T. Brecht, K. Sliwa, B. Abdo, L. Frunzio, S. M. Girvin, R. J. Schoelkopf and D. M. H. *Quantum back-action of an individual variable-strength measurement*. Science **339**, 178–181 (2013).
- [15] S. J. Weber, a. Chantasri, J. Dressel, a. N. Jordan, K. W. Murch and I. Siddiqi. *Mapping the optimal route between two quantum states*. Nature **511**, 570–3 (2014).
- [16] G. de Lange, D. Ristè, M. Tiggelman, C. Eichler, L. Tornberg, G. Johansson, a. Wallraff, R. Schouten and L. DiCarlo. *Reversing Quantum Trajectories with Analog Feedback*. Physical Review Letters **112**, 080501 (2014).
- [17] S. J. Weber, K. W. Murch, M. E. Schwartz, N. Roch and I. Siddiqi. *Quantum trajectories of superconducting qubits*. arXiv preprint arXiv:1506.08165 (2015).
- [18] *Supplementary material*.
- [19] J. Koch, T. Yu, J. Gambetta, a. Houck, D. Schuster, J. Majer, A. Blais, M. Devoret, S. Girvin and R. Schoelkopf. *Charge-insensitive qubit design derived from the Cooper pair box*. Physical Review A **76**, 1–19 (2007).
- [20] H. Paik, D. I. Schuster, L. S. Bishop, G. Kirchmair, G. Catelani, a. P. Sears, B. R. Johnson, M. J. Reagor, L. Frunzio, L. I. Glazman, S. M. Girvin, M. H. Devoret and R. J. Schoelkopf. *Observation of High Coherence in Josephson Junction Qubits Measured in a Three-Dimensional Circuit QED Architecture*. Physical Review Letters **107**, 240501 (2011).
- [21] E. M. Purcell. *Proceedings of the American Physical Society*. Phys. Rev. **69**, 674–674 (1946).
- [22] A. Blais, R.-S. Huang, A. Wallraff, S. Girvin and R. J. Schoelkopf. *Cavity quantum electrodynamics for superconducting electrical circuits: An architecture for quantum computation*. Physical Review A **69**, 062320 (2004).
- [23] N. Bergeal, R. Vijay, V. E. Manucharyan, I. Siddiqi, R. J. Schoelkopf, S. M. Girvin and M. H. Devoret. *Analog information processing at the quantum limit with a Josephson ring modulator*. Nature Physics **6**, 296–302 (2010).
- [24] A. A. Houck, D. I. Schuster, J. M. Gambetta, J. A. Schreier, B. R. Johnson, J. M. Chow, L. Frunzio, J. Majer, M. H. Devoret, S. M. Girvin and R. J. Schoelkopf. *Generating single microwave photons in a circuit*. Nature **449**, 328–331 (2007).
- [25] O. Astafiev, A. M. Zagoskin, A. Abdumalikov, Y. A. Pashkin, T. Yamamoto, K. Inomata, Y. Nakamura and J. Tsai. *Resonance fluorescence of a single artificial atom*. Science **327**, 840–843 (2010).
- [26] A. A. Abdumalikov, O. V. Astafiev, Y. A. Pashkin, Y. Nakamura and J. S. Tsai. *Dynamics of Coherent and Incoherent Emission from an Artificial Atom in a 1D Space*. Phys. Rev. Lett. **107**, 043604 (2011).
- [27] P. Campagne-Ibarcq, L. Bretheau, E. Flurin, A. Auffèves, F. Mallet and B. Huard. *Observing interferences between past and future quantum states in resonance fluorescence*. Physical review letters **112**, 180402 (2014).
- [28] P. Six, P. Campagne-Ibarcq, L. Bretheau, B. Huard and P. Rouchon. *Parameter estimation from measurements along quantum trajectories*. arXiv preprint arXiv:1503.06149 (accepted, 54th IEEE Conference on) (2015).
- [29] J. Gambetta, A. Blais, M. Boissonneault, A. Houck, D. Schuster and S. Girvin. *Quantum trajectory approach to circuit QED: Quantum jumps and the Zeno effect*. Physical Review A **77**, 012112 (2008).
- [30] H. F. Hofmann, O. Hess and G. Mahler. *Quantum control of atomic systems by time-resolved homodyne detection of spontaneous emission*. Phys. Rev. A **57**, 5 (1998).
- [31] H. Amini, M. Mirrahimi and P. Rouchon. *On stability of continuous-time quantum filters*. In Decision and Control and European Control Conference (CDC-ECC) 6242–6247 (IEEE, 2011).
- [32] P. Rouchon and J. F. Ralph. *Efficient Quantum Filtering for Quantum Feedback Control*. Phys. Rev. A **91**, 012118 (2015).